Journal of Asia-Pacific Biodiversity xxx (xxxx) xxx

Contents lists available at ScienceDirect

Journal of Asia-Pacific Biodiversity

journal homepage: http://www.elsevier.com/locate/japb

Original Article

# Identification of seed coat sculptures using deep learning

Gantulga Ariunzaya [a], Jonathan C.L. Kavalan [b], Sungwook Chung [a,*]

[a] Department of Computer Engineering, Changwon National University, Changwon 51140, South Korea
[b] Department of Computer and Information Science and Engineering, University of Florida, Gainesville, FL 32611, USA

ARTICLE INFO

*Article history:*
Received 24 October 2022
Received in revised form
22 November 2022
Accepted 30 November 2022
Available online xxx

*Keywords:*
*Allium* seed coat
deep learning
image recognition
seed coat sculpture

ABSTRACT

Seed coat sculptures, including anticlinal and periclinal walls, are of great taxonomic importance. In this study, we identified seed coat patterns of *Allium* seeds using five deep learning methods namely, CNN, AlexNet, GoogleNet, ResNet50, and VGG16 for the first time. Selected images of seed coat patterns from over 100 *Allium* species reported in previously published literature and data from our samples were classified into seven types of anticlinal (irregular curved, irregular curved to nearly straight, straight, S, U, UO, and omega) and five types of periclinal walls (granule, small verruca, large verruca, marginal verruca, and verrucate verruca). The results revealed that GoogleNet and VGG16 achieved the highest classification accuracy of 90.4% for the anticlinal wall, and VGG16 achieved the highest classification accuracy of 98.1% for the periclinal wall. Moreover, more than three, four, and five methods were combined, and their performance was investigated. Combining more than three methods was the most advantageous. The models achieved a suitable anticlinal wall classification using GoogleNet and periclinal wall classification using VGG16. In conclusion, using the machine-based method, we studied the seed coat of species of *Allium* on our own samples to see if the results of the machine-based method match with the human-based classification.



## Introduction

Seed coat sculptures are of great taxonomic importance in numerous plant groups (Barthlott 1981). In general, there are two types of seed coat sculptures namely, the anticlinal and periclinal walls, and these are often used to characterize taxa, such as species and genus (Barthlott 1981). In the last decade, several researchers have studied the seed coat sculptures of various species and genera of angiosperms (Ghimire et al. 2015; Song and Hong, 2020; Mazur et al. 2022).

The genus *Allium* L. is one of the largest genera in the Amaryllidaceae family with approximately 1000 species that are frequently distributed in the Northern Hemisphere (Choi and Oh 2011). Molecular phylogenies demonstrate the monophyly of *Allium* (Friesen et al. 2006; Li et al. 2010). The recent classifications of *Allium* contain over 780 species and are split into 15 subgenera and 72 sections based on molecular evidence (Friesen et al. 2006). Furthermore, numerous researchers have investigated the seed testa structures of over 400 taxa of *Allium* worldwide (Kruse 1994; Fritsch et al. 2006; Choi et al. 2012; Celep et al. 2012; Duman et al. 2017; Lin and Tan 2017; Veiskarami et al. 2018; Baasanmunkh et al. 2020, 2021). Most studies use the same terminology; however, the seed descriptions are different. For example, there are many types of anticlinal wall undulations (such as S, U, Omega, straight, irregular curved, and nearly irregular curved) and periclinal walls (such as large and marginal verrucae, densely granule, and granule) in *Allium*. However, the anticlinal and periclinal walls of seeds have been identified by humans thus far. In recent years, many researchers have investigated the images of plants including herbaria, leaves, and seeds using deep learning (DL) techniques. However, there are no studies on seed coat sculptures in plants using machine learning (ML) to date.

DL is a type of artificial intelligence that uses computer algorithms based on artificial neural networks that mimic the principles and structure of human neural networks to emulate human cognitive processes (Voulodimos et al. 2018). In DL, there are several Convolutional Network Architectures (CNN) such as AlexNet (Krizhevsky et al. 2017), GoogleNet, VGG16, and ResNetthat use deep learning techniques for image classification. Among these, CNN is widely used in plant science, especially for studying the phenology of plants based on herbaria and photo observation

* Corresponding author. Tel.: +82 55 213 3819.
*E-mail address:* swchung@changwon.ac.kr (S Chung)

Peer review under responsibility of National Science Museum of Korea (NSMK) and Korea National Arboretum (KNA).

https://doi.org/10.1016/j.japb.2022.11.006



Please cite this article as: Ariunzaya G et al., Identification of seed coat sculptures using deep learning, Journal of Asia-Pacific Biodiversity, https://doi.org/10.1016/j.japb.2022.11.006

(Pearson et al. 2020; Piazza et al. 2021; Liu et al. 2022; Reeb et al. 2022). Wagle et al. (2021) classified plant leaves using AlexNet, and tomato leaf diseases using AlexNet, VGG16, ResNet34, EfficientNet-60, and MobileNetV2 (Villaruz 2021; Wagle et al. 2021). Since the advantage of DL methods is the ability to process plant data, researchers are choosing machine-based methods over human-based classification.

In this study, we investigated the seed coat sculptures of *Allium* species using five DL architectures on the data from our samples and those reported in the literature. The DL methods classified each seed wall according to its characteristics. We subsequently divided the data into test and training data and trained the CNN, AlexNet, GoogleNet, VGG16, and ResNet50 architectures using 50 iterations.

## Material and methods

This study classified *Allium* seed coats using various algorithms. Our proposed algorithm is presented in Figure 1.

### *Dataset*

We selected the seed coats of over 100 *Allium* species from previous studies (Celep et al. 2012; Choi et al. 2012; Duman et al. 2017; Veiskarami et al. 2018; Baasanmunkh et al. 2020). Tables 1 and 2 list the details of the dataset used in this study. The seed coat sculptures of *Allium* species are displayed in Figure 2.

### *Data preprocessing*

In this section, the data preprocessing method is described; this is a crucial step before building the models. The aim of preprocessing is to enhance the images and remove unwanted deformation (Golnabi and Asadpour 2007). Achieving good results from the applied models in ML and DL projects requires a full understanding of the problem, data collection, and environment. Therefore, the data resources of the collective images of the *Allium* seed coat sculptures obtained using scanning electron microscopy (SEM) must be preprocessed before decomposition, and our preprocessing method consisted of two parts: anticlinal and periclinal wall detection sections.

### *Anticlinal wall detection*

Our study on detecting the strategic architectural lines of the anticlinal walls using an algorithm is illustrated in Figure 3. For the first pre-processing, the goal is, we crop the seed walls separately. The initial step was to convert the images to grayscale. The image data was reduced from three-dimensional to one-dimensional data (Cadík 2008), which formed the basis for the next step. The color image (RGB) was converted to a grayscale image with grayscale value in the range of 0 and 255 (Horng et al. 2005). This is the simplest and most common technique of computer vision and object detection. After converting the images to grayscale, we applied an adaptive threshold to yield binarized images. The images were segmented based on this adaptive threshold that makes the proposed method adaptable to image quality and facilitates noise removal (Bradley and Roth 2007). Furthermore, computes the average background illumination to display the local threshold image (Davies 1990). In the next stage, a locally adaptive threshold was applied to the binarized images to create a binary image from the original image according to the threshold. Similar to the locally adaptive threshold, this stage creates binarized images by calculating the threshold per pixel using local mean intensity in the neighborhood of the pixel (Cadík 2008). The threshold values are 1 (white) and 0 (black) (Dev et al. 2016; Khalifa et al. 2021). In this study, we selected a threshold value of 0.6 that is suitable for data

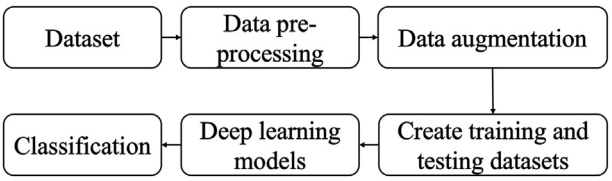


**Figure 1.** Proposed algorithm.

preprocessing to ensure that the objects can be detected. The pixel values greater than 0.6 represent the seed coat pattern in white, while the rest represent background pixels. Subsequently, we implemented a label connected component technique on the binary images. This technique identifies and combines the labels of the connected components in an image (He et al. 2009). Haralick and Shapiro (1992) reported that the connected component label returns a matrix which contains the connected component the same input labels as the image. By doing this, the pixels labeled 0 corresponds to the background and labeled 1 indicates foreground object. These pixels belong to the same object if they are neighbors. Also, gives you the membership of each pixel. Therefore, this tells you where each pixel belongs to if falls on an object. In our study, the seed coat present in the image can be identified by the number of objects found in the labeled connected components. In the final stage of preprocessing, we measured a set of properties for each region in the binary image. The bounding box and area of properties using these measurements are computed in the implementation stage, in which we obtained the location of the objects in the images. An area was represented by the initial number of pixels in the region and the bounding box was the smallest rectangle containing this area (Huang and Wang 1995). After preprocessing, the images were immediately transferred to the feature extraction step followed by the classification process.

### *Periclinal wall detection*

With the help of the anticlinal wall pre-processing architecture, we aimed to detect the periclinal wall. Figure 4 illustrates the algorithm for detecting the periclinal walls. First, the input image was used only to identify the objects. Herein, we obtained a mask where the region in the image was solid. Then we fill in the hole in the input binary image. This creates another binary image extracting all connected components with the area specified in binary image. It also returns a binary that contains only objects that meet the output value criteria. After, we aim to get to the foreground area. The binarized images consist of a white foreground and black background (Huang and Wang 1995; Singh et al. 2012). In the next stage, the mask was applied to the original image and the region outside the mask was erased, thereby masking the object from the original image that is the foreground area. Otherwise, is the background area, which is also an unwanted area in this section. Next, we converted the masked image to a grayscale image, i.e. we

**Table 1.** Abbreviations of the anticlinal and periclinal seed types.

| Anticlinal wall | | Periclinal wall | |
|---|---|---|---|
| Original name | Abbreviation | Original name | Abbreviation |
| Irregular curved | IC | Granule | GT |
| Irregular curved to nearly straight | INS | Large verruca | LT |
| Omega | O | Marginal verruca | MT |
| U | U | Small verruca | ST |
| U to omega | UO | Verrucate | VT |
| S | S | | |
| Straight | ST | | |

Please cite this article as: Ariunzaya G et al., Identification of seed coat sculptures using deep learning, Journal of Asia-Pacific Biodiversity, https://doi.org/10.1016/j.japb.2022.11.006

**Table 2.** Details of the dataset in this study.

| Sample | Classes | Original image size | Normalized image |
|---|---|---|---|
| Anticlinal wall | 7 | 1228 × 1108 | 150 × 150 |
| Periclinal wall | 5 | 1228 × 1108 | 150 × 150 |

converted the RGB image to grayscale. (McAndrew 2004; Kanan and Cottrell, 2012) reported that converting an RGB image to grayscale impacts the performance during image recognition. However, this is the simplest method of image recognition, pattern recognition, and computer vision, and this was the basis of the next stage of data preprocessing. We then calculate the local variable threshold of sensitivity using the scalar coefficient of the scalar form in the region [0, 1], and express the sensitivity of splitting two more pixels in foreground. This function chooses a threshold based on the local mean intensity value of each pixel neighborhood. The values greater than 0.6 pixels indicate the seed coat pattern in white, while others represent background pixels. Then we convert the image to a binary image by specifying this threshold. After we applied label connected component to the binary image. It returned label connected component matrix, containing the labels for object in the input image. The purpose of the final stage was to visualize the color assigned to each object based on the number of objects in the label matrix. After preprocessing, the images were immediately passed on to the feature extraction stage followed by the classification process.

*Data augmentation*

Data augmentation is a very useful method for preventing the issues caused by limited data, and data growth facilitates this by efficiently using existing data (Antoniou et al. 2017; Shorten and Khoshgoftaar 2019). Each image was repeated six times during the model training process according to the following criteria: rotation, height shift, width shift, and zoom ranges (Table 3).

The rotation operation was rotated image right or left on an axis between 1° and 359°, thereby changing the position of the object in the frame (Antoniou et al. 2017; Iwana and Uchida 2021; He et al. 2021; Khalifa et al. 2021). In this study, the rotation range was 5; therefore, the original image was rotated by 5°. In the next data augmentation method, the height shift range was shifted from top to bottom by 0.05 pixels. Next, the width shift range was shifted from left to right by 0.05 pixels. Finally, the image was zoomed by 0.1 pixels. Figure 5 illustrates data augmented images.

*Creating the training and testing dataset*

Splitting the training and testing datasets are important for training the models. A common strategy is labeling the data and splitting it into training and validation sets into 70–80% for training and 20–30% for validation (Abbas et al. 2021; Wagle et al. 2021). The ML and DL fields use the training data to train models to identify patterns and validate the data to evaluate the predictability of the trained model. After preprocessing, our dataset comprised a

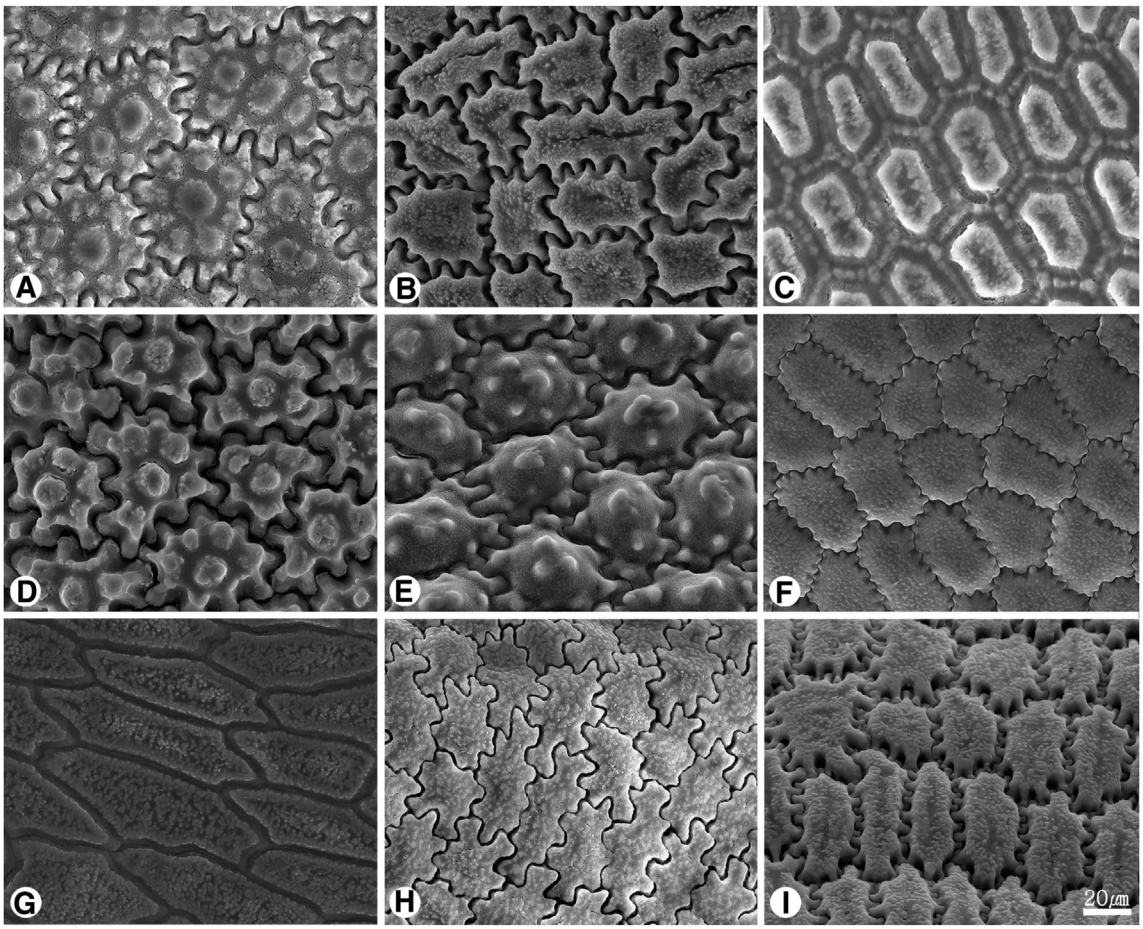


**Figure 2.** Seed coat sculptures of *Allium* species reproduced from (Baasanmunkh et al. 2020): A, *A. filidens*; B, *A. caesium*; C, *A. carolinianum*; D, *A. caeruleum*; E, *A. svetlanae*; F, *A. vodopjanovae*; G, *A. ramosum*; H, *A. anisotepalum*; I, *A. pallasii*.

Please cite this article as: Ariunzaya G et al., Identification of seed coat sculptures using deep learning, Journal of Asia-Pacific Biodiversity, https://doi.org/10.1016/j.japb.2022.11.006

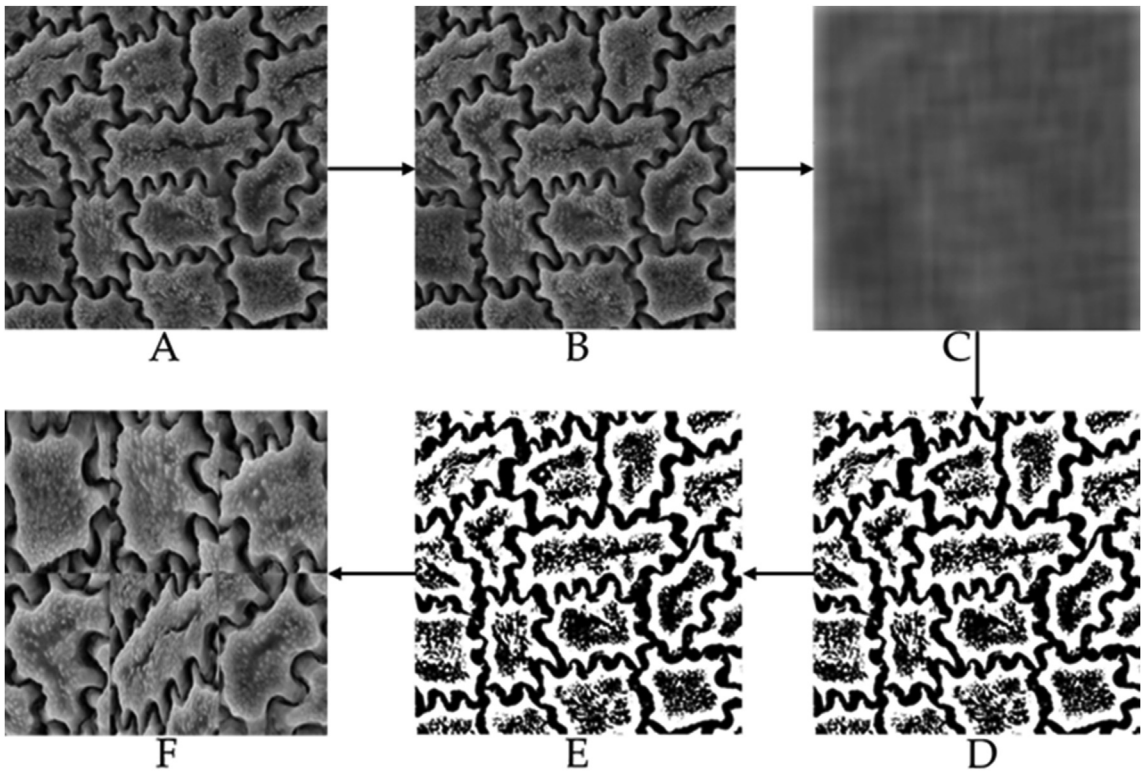


**Figure 3.** Data preprocessing of the images of the anticlinal walls: A, input image; B, grayscale image; C, threshold using adaptive thresholding; D, binary image; E, labeled image; F, and preprocessed image.

total of 31,759 seed coat images. The preprocessed dataset was then split by 70/30 to form the training and testing datasets.

*DL models*

In this study, we aimed to create a computationally efficient method for classifying seed coats. The input of the classification stage was the categorical metadata associated with the images, and the classes were considered to be species. We used five architectures namely, CNN, AlexNet, GoogleNet, VGG16, and ResNet50, to classify the *Allium* seed coat sculptures from the image data. Each network can categorize these images according to certain characteristics. In DL, the most common network is CNN that consists of a convolution layer, pooling layer, and fully connected layer. AlexNet is designed to provide state-of-the-art recognition accuracy to ML and computer vision recognition. This model has 5 convolutional

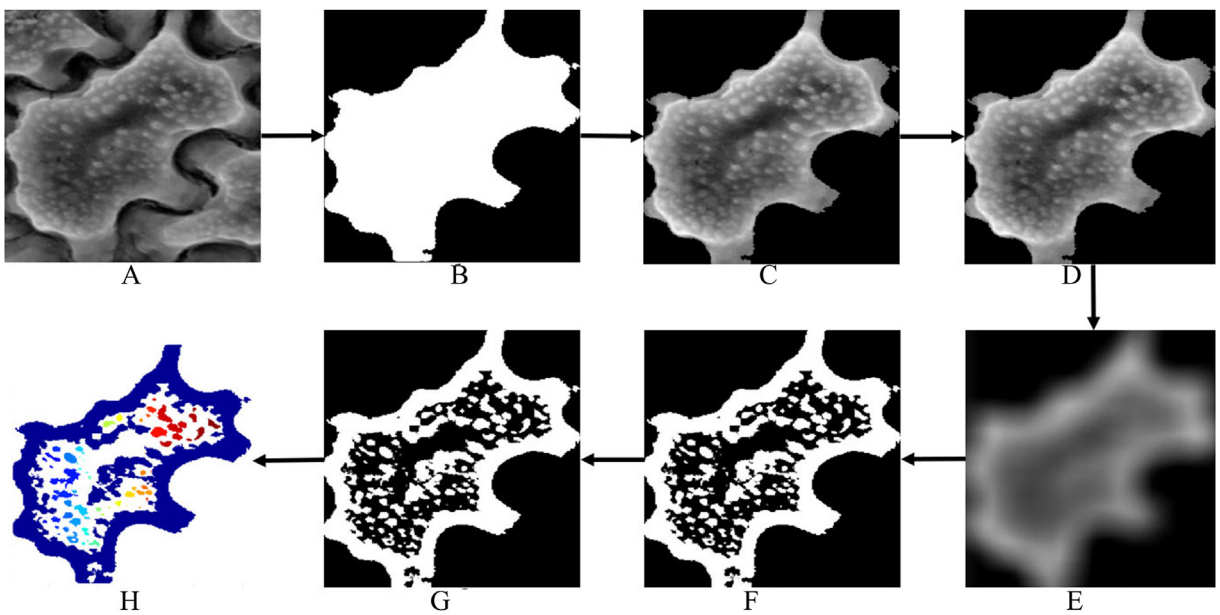


**Figure 4.** Data preprocessing of the images of the periclinal walls: A, Input image; B, Binary threshold image; C, Masked image; D, Grayscale image; E, Binary image obtained by using an adaptive threshold; F, Binary image; G, Labeled image; H, And preprocessed image.

Please cite this article as: Ariunzaya G et al., Identification of seed coat sculptures using deep learning, Journal of Asia-Pacific Biodiversity, https://doi.org/10.1016/j.japb.2022.11.006

**Table 3.** Details of the dataset.

| Dataset | Augmentation technique | Original dataset | Data augmented dataset |
|---|---|---|---|
| Anticlinal wall<br>Periclinal wall | Rotation = 5<br>Width_shift_range = 0.05<br>Height_shift_range = 0.05<br>Zoom_range = 0.1 | 770 | 31,759 |

layers, 3 max-pooling layers, 2 normalization layers, 2 fully connected layers, and 1 softmax layer (Krizhevsky et al. 2017). Also, each convolutional layer is related of convolutional layers and ReLu nonlinear activation function. After the evolution of AlexNet, the Visual Geometry Group at Oxford University proposed VGG16 which is an accurate assessment of in-depth networks using proposed architecture with very small 3 × 3 convolutional filters. GoogleNet contains 22 layers deep, with 27 pooling layers included. The network is built with many deep layers; there may be a problem of overfitting. To solve this problem, the authors of the study "Going Deeper with Convolutions" proposed a GoogleNet architecture with the intention of having multiple sizes of filters that can work at the same level. With this idea, the network is not deeper but wider. In particular, the ResNet50 network is deeper than previous networks. This can create an identity block with a shortcut connection that skips one or more layers in a basic multilayer structure.

To optimize each model for the dataset, we tuned its hyperparameters by changing the learning rate and optimizer. The batch size was determined based on the sample size of each database. In the models that predict the distribution of multinomial probabilities, the softmax function was used as an activation function in the output layer (Banerjee et al. 2020). More precisely, softmax is a multi-class classifier; and one optimizer was considered in this study. The Adam optimizer is a replacement algorithm for stochastic gradient descent that combines the best properties of AdaGrad and RMSProp to provide an optimization algorithm that can handle sparse gradients in noisy problems, which is the most common option in DL. Categorical cross-entropy, which is known to be suitable for classification, was used as a function to reduce loss or the difference between the actual and predicted values. Each model was trained using a learning rate of 0.0001, a batch size of 64, Adam hyperparameter optimizer, and 50 iterations. The hyperparameter tuning for each model are listed in Table 4. Finally, the classification models were tested using the test datasets that were not used in the construction of the classification models. All the models were implemented with the Python programming language in a Tensor Flow framework on a PC equipped with the Intel Xeon SPS-4208/2.1Ghz-11M-8C * 2EA memory of 128B(16GB*8EA) RED4-2983 Max 16s/2TB.

### *Combined models*

After the classifications, we attempted to combine the two models for detecting anticlinal and periclinal seed coat sculptures. Figure 6 illustrates the proposed combined model algorithm. The first step in our proposed algorithm is to obtain models such as CNN, AlexNet, VGG16, GoogleNet, and ResNet50. Herein, the anticlinal walls show the boundary of the seed coat. After doing this, we set out to obtain a model for each periclinal wall network. We then used a test image to test the combined model. This was followed by the combination of the anticlinal and periclinal wall models, when the two walls were connected, one seed of information appeared. Therefore, we can use the results with the help of a combined model.

## Results and discussion

In this study, we identified the seed coat sculptures of over 100 *Allium* species using five DL methods. Each training test is explained in the sections below.

### *Comparison of the model performances*

The training accuracy is displayed in Figure 7. The accuracies for training the models using the anticlinal wall were 79% for CNN, 87.7% for AlexNet, 62.1% for VGG16, 90.4% for GoogleNet, and 88.3% for ResNet50. The accuracies for training the models using the periclinal wall were 55.3% for CNN, 73.5% for AlexNet, 98.1% for VGG16, 87.6% for GoogleNet, and 96.4% for ResNet50. The highest accuracy of training the anticlinal wall models was 90.4% for GoogleNet. In contrast, the lowest accuracy was 62.1% for the VGG16 architecture. The highest accuracy for training the periclinal wall models was 98.1% for the VGG16, whereas the lowest training accuracy was 55.3% for the CNN architecture.

### *Identification of the anticlinal wall using each model*

In Table 5, we summarize the results for the anticlinal wall procedure compared to the results provided by machine-based and human-based classifiers. If we look at the results of the AlexNet architecture, we can see that the results of the anticlinal wall type are relatively different. In the case of the IC type, the predicted percentage applies to types other than the IC type. These include U-8.3%, S-41.2%, and ST-50.5%. The ST type achieved higher prediction percentages than those of other types. The ST type matched prediction result is 48.7%. For the INS- type, does not have matched results but related to other types. These include U-2.3%, UO-0.9%, S-28.9%, and ST-67.9%. In this case, prediction result of ST - type achieved high prediction. The O type prediction is predicted into U-7.5%, UO-12.5%, S-8.1%, and ST-71.9%. Also, O type does not include results here. Similarly, INS and IC type, in this case, ST achieved higher prediction percentages than those of the other types. Conversely, in the U type, only 10% of images were assumed to belong to the correct class. More precisely, the results of this type belong to different types, and it can be seen that 4.2% of the prediction belong to the UO- type. For the S type, the correct prediction was 28.6%, and for ST, the correct classification was 48.7%. In this case, all the testing set in ST had the highest accuracy.

As listed in Table 5, CNN is the correctly predicted ST type sample. In contrast, the IC, INS, and O - types are assumed to belong to different classes. Additionally, 2.1%, 18.5%, and 100% were predicted for the U, S, and ST types. AlexNet and CNN's performance predictions have the highest percentage of ST, but CNN architecture predictions are higher than AlexNet architecture. Next, we report the results of GoogleNet. GoogleNet and CNN defined ST type with high accuracy. IC, INS, and U types are also classified into different categories. These include U-21.5%, UO-44%, and S-18.5% were identified correctly. The UO type was identified with 44% higher accuracy than the CNN and AlexNet classifiers. Also, as in previous architectures, there are no IC and INS - types.

Please cite this article as: Ariunzaya G et al., Identification of seed coat sculptures using deep learning, Journal of Asia-Pacific Biodiversity, https://doi.org/10.1016/j.japb.2022.11.006

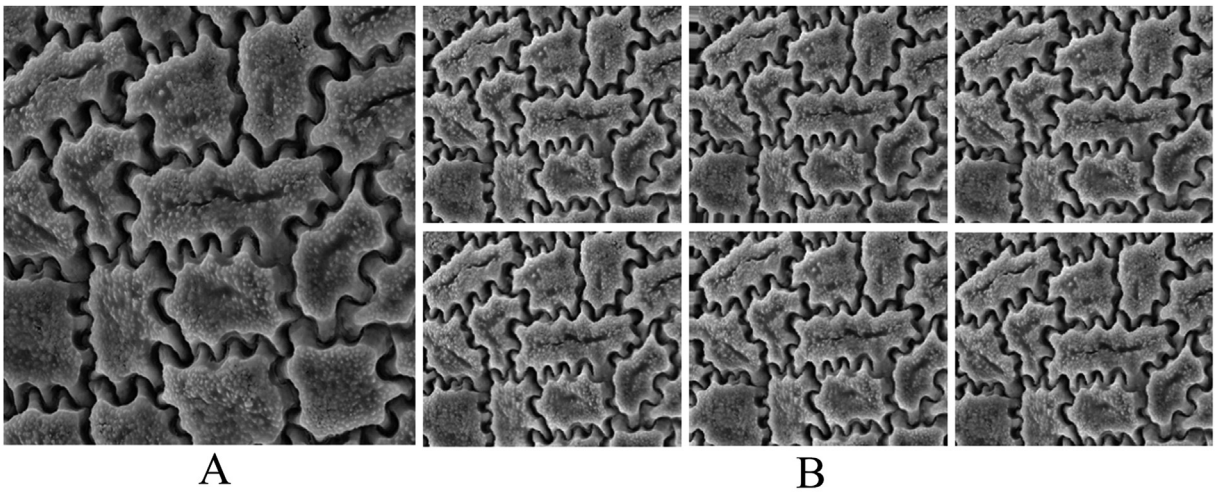


**Figure 5.** Example of the augmented images of *A. pallasii*: A, the original image; B, augmented images.

Next, we discuss the results of ResNet50. As shown in Table 5, the highest classified type is ST, similar to the results of CNN and GoogleNet. Previous models did not predict the O - type. Furthermore, the prediction of O was 10% higher than those in AlexNet, CNN, and GoogleNet. ResNet50 and CNN equally defined the U - type as 2.1%, but lower than GoogleNet prediction.

Finally, we summarize the VGG16 results. The results of the ST classification were the same as those of AlexNet, CNN, GoogleNet, and ResNet50. Predictions for IC and INS are related to different classes. Additionally, 11.3% of O was correctly classified, which was 1.3% higher than the results obtained from ResNet50. U was classified with 15.2% lower accuracy than that obtained from ResNet50 and 6.3% lower than that obtained from GoogleNet.

Therefore, ST achieved the highest percentage of correct prediction. Otherwise were classified into different types.

### *Identification of the periclinal wall using each model*

In Table 6, the results of classifying the periclinal walls using the models and machine-based classifiers are listed.

For AlexNet, all images of GT - type are well classified as GT (82%) among the five types. Whereas LT type is identified as VT (77.8%), followed by VT type as GT (58.4%), MT as GT (31.4%) and as LT (45.4%). For the CNN, GT and VT types are correctly classified. This case is more predictable than AlexNet classifier. For the MT type, predictions were divided into different classes. The correct classification percentage of LT was 16.1%, but otherwise related to other classes. This was higher than the results obtained from AlexNet. ST was not correctly classified but was divided into different classes. Finally, the correct classification of VTs was fully consistent and higher than the results of AlexNet by 88.4%.

**Table 4.** Optimized hyperparameters for model advancement.

| Hyperparameter | Value | | | | |
|---|---|---|---|---|---|
| | CNN | AlexNet | GoogleNet | ResNet50 | VGG16 |
| Batch size | 64 | | | | |
| Optimizer | Adam | | | | |
| Activation function | ReLu | | | | |
| Learning rate | 0.0001 | | | | |
| Epoch | 50 | | | | |
| Loss function | Categorical cross-entropy | | | | |

Next, we discuss the GoogleNet predictions. The VT type is well classified as VT-92.8% among the five types. While GT-43.4%, MT-2.9%, LT-16.1%, and ST-17.8% were classified.

Next, we discuss the results of the ResNet50 classification. The GT prediction is similar to the prediction in the results of AlexNet. Only 50.7% of MT were correctly classified, which is 47.8% higher than the results of GoogleNet and 46.1% higher than the results of AlexNet. More than 4% of LTs were classified correctly, and this was 11.7% lower than the results of GoogleNet. The correct prediction percentage for ST was 11.2%; this was 6.6% lower than the results of GoogleNet. This was also 9% higher than the results of AlexNet. Finally, the predicted percentage of VT was 51.7%, which was lower than the GoogleNet classifier.

Lastly, we discuss the results of the VGG16 classifier. VGG16, like CNN and ResNet50, correctly predicted GT. Only 28% of MT were classified correctly, and otherwise distinguished into different categories. For LTs, 19.8% fit the correct class, and this was 15.3% higher than the results of ResNet50. Only 33.8% of ST was correctly classified, and this was 17.5% higher than the results of AlexNet, and 24.1% higher than the results of ResNet50. Overall, 13.5% of VT was correctly classified.

### *Results of the combined models*

In Table 7, we show detailed classification of the combined model. In AlexNet classification, the original types of U-VT, U-LT, U-MT, O-VT, O-MT, UO-LT, S-GT, S-VT, and S-LT are classified as IC-GT - 100%. IC-GT was predicted with (59%) accuracy. The O-LT (18%), INS-GT (20%), ST-GT (45%), and ST-MT (50%) predicted to be IC-GT. In addition, UO-GT, UO-VT, and ST-LT classified to ST-VT (100%). In contrast, U-GT, ST-VT, and ST-ST are classified as S-ST with different percentage. However, only INS-GT was recognized as O-MT with (60%) accuracy.

In CNN approach, most of the types were assumed to be IC-GT, as shown by the results of AlexNet. These include U-VT, U-GT, U-LT, U-MT, UO-GT, UO-VT, and S-GT. Only 100% of the S-VT was assigned to the O-MT. O-MT, UO-MT, INS-GT, S-LT, ST-GT, ST-VT, ST-ST, ST-LT, and ST-MT types were classified to the ST-VT. Overall, about 51% of the IC-GT had classified to the S-ST. Among type of O-LT had the medium percentage of images classified (48%). In UO-LT, identification was with 96% of the different assignations. Thus, CNN has higher predictability than the previous model.

Please cite this article as: Ariunzaya G et al., Identification of seed coat sculptures using deep learning, Journal of Asia-Pacific Biodiversity, https://doi.org/10.1016/j.japb.2022.11.006

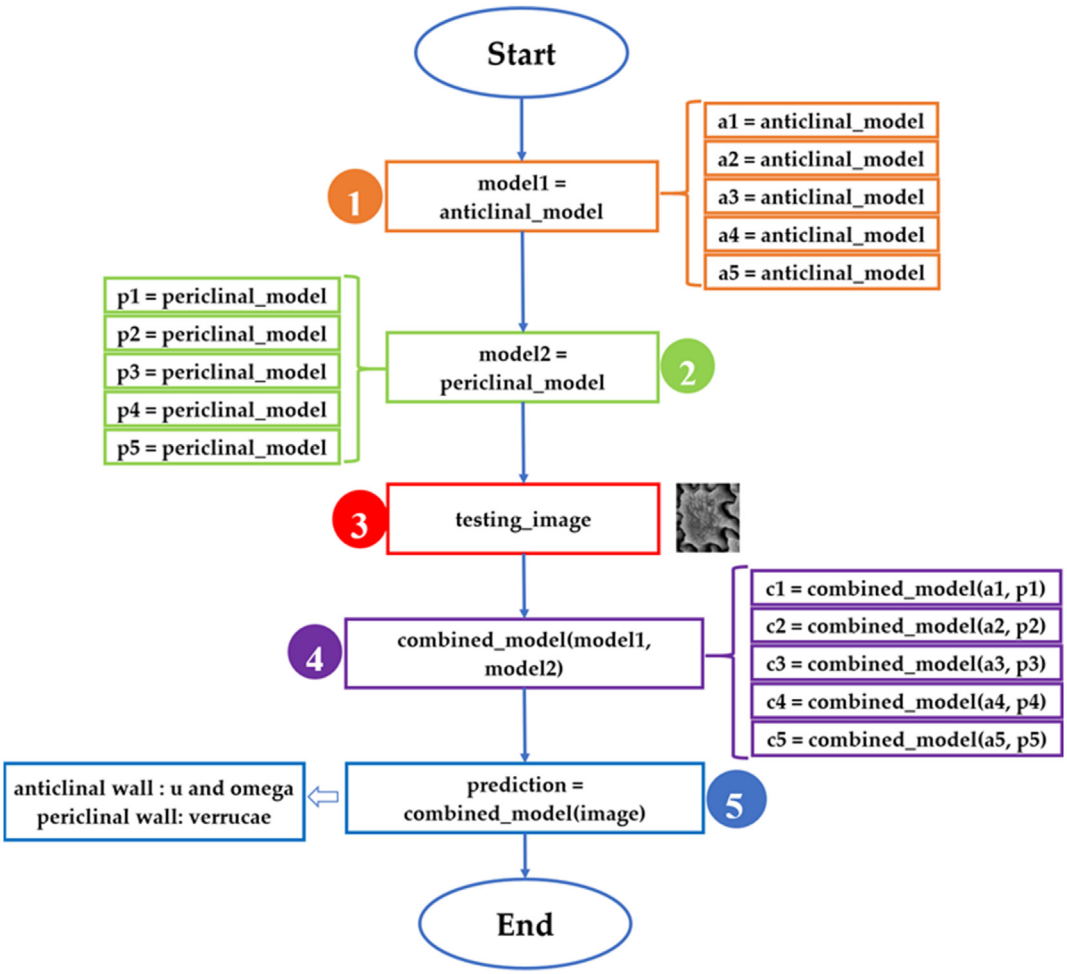


**Figure 6.** Proposed combined algorithm.

Next, we discuss the results based on GoogleNet. Similarly, AlexNet and CNN, most identifications were IC-GT. These include U-VT, U-GT, U-LT, U-MT, IC-GT, O-VT, O-MT, UO-GT, UO-VT, UO-LT, UO-MT, S-GT, S-VT, S-LT, ST-GT, ST-VT, ST-ST, ST-LT, and ST-MT. Both AlexNet and CNN did not classify to the O-MT. In GoogleNet approach, predicted O-MT (30%) is higher than previous models. In INS-GT, predict different approach S-ST (20%).

Next, we combine the data of the two walls obtained from ResNet50. More types are covered than the predictions of previous models. These include IC-GT, O-VT, O-MT, S-GT, S-ST, S-VT, S-LT, ST-VT, ST-LT, and ST-MT. In the previous tables, most of the IC-GTs predicted different approaches, whereas, in this section, most types of O-MT were predicted correctly. The U-VT, O-LT, O-MT, UO-GT, UO-LT, UO-MT, INS-GT, S-GT, S-VT, ST-GT, ST-VT, and ST-MT types were classified to the O-MT with different percentage. In addition, 75% of IC-GTs was classified as IC-GT, U-MT was classified as S-ST (100%), the O-VT was classified as O-MT.

Finally, we summarized the results of the VGG16 method for the combined data of the two walls. S-LT (100%), ST-GT (50%), ST-VT (100%), ST-ST (100%), ST-LT (100%), and ST-MT (50%) predicted to be ST-VT. For U-VT, U-LT, and UO-LT were predicted to be S-VT with 100% prediction. UO-MT was predicted to be ST-ST (49%). From these, the aggregated results predicted that most of the types were IC-GT, ST-VT, and O-MT.

*DL for detecting the anticlinal walls*

In Table 8, we list the datasets used in this study. As shown in Figure 8A, in more than three methods, the ST type is correctly identified as the ST type, which is suitable for both human and machine-based recognition. In contrast, O and U images were not assigned to the correct classes and the recognition rate was 0%. Overall, approximately 48.6% of the S type images and 21.6% of the UO type images were correctly classified. In addition, the S-type images were predicted as STs with 27.3% accuracy, UOs were predicted with 15.8% accuracy, and Us were predicted with 8.3% accuracy. Furthermore, only 0.8% of the INS images and 0.3% of the IC images were assigned to the correct class. For INS, 65% were assumed to be S and 34.2% were assumed to be ST. This proved that the machine-based method confused the INS seed wall with the S and INS seed walls. For the IC seed walls, 69% was classified as the S-type, 25.1% as ST, 5.2% as O, and 5.4% as U. Next, 11.7% of UO was classified as S, 27% as ST, and 21.6% as UO. O was classified as 17.1% S, 24.7% ST, 35.2% UO, and 22.5% U. Finally, U was classified as 10.6% UO, 15.3% O, and 0.6% S. This proved that the UO, O, and U-type seed walls were confused by the models because they appear similar. The machine-based method also predicted that the ST-type seed wall was undoubtedly ST.

In Figure 8B, we show the results of more than four methods. The ST was also predominant in this case (81.9%). The S of the

Please cite this article as: Ariunzaya G et al., Identification of seed coat sculptures using deep learning, Journal of Asia-Pacific Biodiversity, https://doi.org/10.1016/j.japb.2022.11.006

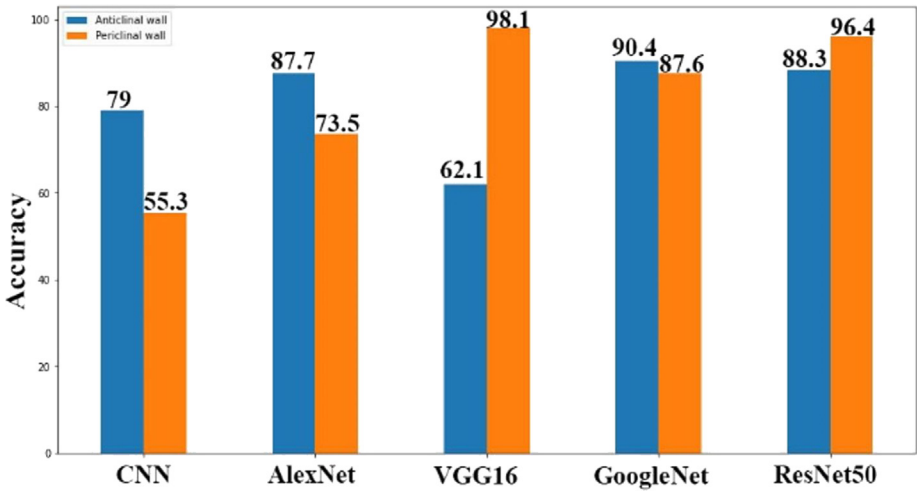


**Figure 7.** Accuracy of CNN, AlexNet, VGG16, GoogleNet, and ResNet50 for the classification of anticlinal and periclinal walls.

(20.4%) images were identified correctly, (32.9%) were identified as the INS, and (25.1%) as the IC. This suggested that the machine-based methods confuse the S, INS, and IC-types. For other types, predictions were 0% and it is also possible classification.

In Figure 8C, we show the results of combined more than five methods. However, the categories shown in Figure 8B are similar to those in Figure 8C. This indicates that the ST continues to dominate the other types with more than five methods and 17.9% of entire models. However, the S is still matching for the other models. These include S, INS, and IC.

*DL for detecting periclinal walls*

The results of detecting the periclinal walls are displayed in Figure 9. Firstly, the results of combining more than three methods are illustrated in Figure 9A. Among all the types, GT had the highest percentage of images correctly classified (81.9%), and 70.1% of VT was correctly identified. Additionally, 2.6% of GT was classified as MT, 0.1% as ST, and 0.1% as VT. The majority of VTs were classified as MTs (47.8%), STs (17.5%), LTs (32.2%), and VTs (70.1%). Additionally, 2.7% of MTs were classified correctly and 0.3% was assigned to ST. STs were classified as GTs (1.2%), MTs (0.5%), STs (1.8%), and VTs (17.5). The LT seed walls were classified as STs (2.1%) and VTs (32.2%). Finally, VTs were classified as MTs (10.2%), STs (2%), and VTs (70.1%). From these results, we concluded that most of the seed walls were being confused with the VT seed walls.

Secondly, Figure 9B shows the results of combining more than four methods. This shows that the GT has 43% recognition. Similar to the previous Figure 9A, most seed walls were considered to be VT, and 2.6% of GT were considered to be VT. In addition, 11.7% of LT is predicted to be VT, and also 61.1% of VT is highly considered to be VT. Only 0.6% of the images of ST were assigned to the correct class, and MT was classified as about 0.4% MT.

Thirdly, Figure 9C illustrates the results of combining more than five methods. VT was also dominantly predicted here with a recognition percentage of 24.7%. In addition, the recognition rate of LT was 5.4% of VT. This suggested that VT was more predictable than the other seed walls. However, LT was confused with the VT seed wall.

*Combined model results*

Next, we discuss the combined model results from Figure 10. The results of the anticlinal wall detection are shown in Figure 8 and those of the periclinal wall detection are shown in Figure 9. The results of combining more than three methods are shown in Figure 10A. Additionally, Table 9 lists the datasets used in our combined models. Here, 100% of U-GTs, 100% of U-VTs, 100% of U-

**Table 5.** The SEM images of the anticlinal walls classified using the five models (accuracy in percentages). The matched results are clearly highlighted.

AlexNet results

| | IC | INS | O | U | UO | S | ST |
|---|---|---|---|---|---|---|---|
| **IC** | | | | 8.4 | | 41.2 | 50.4 |
| **INS** | | | | 2.3 | 0.9 | 28.9 | 67.9 |
| **O** | | | | 7.5 | 12.5 | 8.1 | 71.9 |
| **U** | | | 7.5 | **10** | 1.3 | 14.1 | 67.1 |
| **UO** | | | 12.5 | 7.4 | **4.2** | 14.7 | 61.2 |
| **S** | | | | 3.5 | | **28.6** | 67.9 |
| **ST** | | | | 1.4 | 11.1 | 38.8 | **48.7** |

CNN results

| | IC | INS | O | U | UO | S | ST |
|---|---|---|---|---|---|---|---|
| **IC** | | | | 12.5 | | 12.6 | 74.9 |
| **INS** | | | | | 33.1 | | 66.9 |
| **O** | | | | 12.3 | | | 87.6 |
| **U** | | 0.4 | | **2.1** | 25.3 | 25.1 | 47.1 |
| **UO** | | | | 3.5 | | | 96.5 |
| **S** | | | | 3 | | 18.5 | 78.6 |
| **ST** | | | | | | | **100** |

GoogleNet results

| | IC | INS | O | U | UO | S | ST |
|---|---|---|---|---|---|---|---|
| **IC** | | | | 4.1 | | 8.5 | 87.4 |
| **INS** | | | | 33.1 | | | 66.9 |
| **O** | | | | | 22.8 | | |
| **U** | | 12 | | 21.5 | 7.8 | 18.5 | |
| **UO** | | | 33.1 | | 44 | 2.5 | |
| **S** | | 8 | | 28 | 16.7 | 18.5 | |
| **ST** | | | | | | | **100** |

ResNet50 results

| | IC | INS | O | U | UO | S | ST |
|---|---|---|---|---|---|---|---|
| **IC** | | | | | | | 100 |
| **INS** | | | | | | | 100 |
| **O** | | 25.7 | **10** | 18.1 | 6.7 | 5.2 | 34.3 |
| **U** | | 0.4 | | **2.1** | 25.3 | 25.1 | 47.1 |
| **UO** | | | | **3.5** | | | 96.5 |
| **S** | | 14.5 | 3.3 | 6.8 | | | 75.4 |
| **ST** | | | | | | | **100** |

VGG16 results

| | IC | INS | O | U | UO | S | ST |
|---|---|---|---|---|---|---|---|
| **IC** | | | | | | | 100 |
| **INS** | | | | | | | 100 |
| **O** | | | **11.3** | 5.9 | 1.9 | 18.2 | 62.7 |
| **U** | | | 10.7 | **15.2** | 2.9 | 18.3 | 52.9 |
| **UO** | | | 8.8 | 10.9 | | 13.6 | 67.1 |
| **S** | | 15.2 | | 7.3 | 2.4 | | 75.1 |
| **ST** | | | | | | | **100** |

Please cite this article as: Ariunzaya G et al., Identification of seed coat sculptures using deep learning, Journal of Asia-Pacific Biodiversity, https://doi.org/10.1016/j.japb.2022.11.006

**Table 6.** The SEM images of the periclinal walls classified using five models (accuracy in percentages). The matched results are indicated by bold.

| AlexNet results | | | | | | CNN results | | | | | | GoogleNet results | | | | | | ResNet50 results | | | | | | VGG16 | | | | | |
|---|---|---|---|---|---|---|---|---|---|---|---|---|---|---|---|---|---|---|---|---|---|---|---|---|---|---|---|---|---|
| | GT | MT | LT | ST | VT | | GT | MT | LT | ST | VT | | GT | MT | LT | ST | VT | | GT | MT | LT | ST | VT | | GT | MT | LT | ST | VT |
| GT | **82** | 1.3 | | 1.8 | 14.9 | GT | **100** | | | | | GT | **43.4** | 3.1 | | 4.6 | 48.9 | GT | **100** | | | | | GT | **100** | | | | |
| MT | 31.4 | **4.6** | 45.4 | 16.3 | 2.3 | MT | 31.8 | | | | 68.2 | MT | 28.7 | **2.9** | | 1.4 | 67 | MT | | | **50.3** | 3 | 2.6 | 44.1 | MT | 16.5 | **28** | 47.6 | | 7.9 |
| LT | 1 | 7.1 | | 14.1 | 77.8 | LT | 32.2 | | **16.1** | 12.9 | 38.8 | LT | 32.2 | | **16.1** | 12.9 | 38.8 | LT | 20.2 | 42.3 | **4.5** | 8.1 | 24.9 | LT | | 19.8 | | | 80.2 |
| ST | 1.8 | 16.3 | 7 | **2.2** | 8 | ST | 36.9 | 11.2 | 25.7 | | 26.2 | ST | 11.4 | 24.1 | 0.4 | **17.8** | 46.3 | ST | 56.6 | 28.9 | | **11.2** | **3.3** | ST | 12.2 | 24.6 | | **33.8** | 19.4 |
| VT | 58.4 | 16.4 | 5.6 | 8 | **11.6** | VT | | | | | **100** | VT | | 2.6 | | 4.6 | **92.8** | VT | 46.8 | | | | **51.7** | VT | 58.4 | 27.7 | | 0.4 | **13.5** |

LTs, 100% of U-MTs, 100% of IC-GTs, 20% of IC-MTs, 13.3% of INS-GTs, 15.3% of O-VTs, 24% of O-LTs, 37.3% of S-VTs, 100% of UO-GTs, 17.3% of UO-VTs, 42% of UO-LTs, and 100% of UO-MTs were classified as IC-GT. Similarly, 13.6% of UO-VTs, 30.4% of UO-LTs, 30.4% of UO-MTs, and 100% of ST-LTs were assumed to be ST-LTs, whereas 4% of S-LTs, 6.1% of ST-GTs, 37.6% of ST-STs, 80.4% of ST-MTs, and 12% of UO-GTs were assumed to be ST-STs. O-MTs were projected as 9.3% S-LTs. For ST-LTs, UO-VTs were predicted at 13.5%, UO-LTs at 30.4%, and UO-MTs at 30.4%. Here, 100% of S-GTs were assumed to be INS-GTs. From this, IC-GT was predicted with 100% accuracy. At a low rate, ST-ST was rated correctly at 37.6% and ST-LT was rated correctly at 13.5%.

Figure 10B shows the results of combining more than four methods. Here, 20% of U-GTs, 86.7% of U-VTs, 50% of U-LTs, 66.7% of U-MTs, 80% of IC-GTs, 8% of O-VTs, 16.7% of S-VTs, 13.3% of UO-LTs, and 83.3% of UO-MTs were classified as IC-GTs. Similarly, 26% of ST-MTs and 6.5% of UO-VTs were assumed to be ST-LTs. S-GTs were assumed to be INS-GTs with an accuracy of 28%.

For more than five methods, there are no interrelated values in these results. All the values may be zero from the previous two experimental results.

## *Discussion*

Herein, we compared the classification of seed coat sculptures by humans and machines. A database containing 31,759 augmented images of anticlinal and periclinal walls of *Allium* seed coats were used in this study. The main contribution of this study was to determine the suitable machine-based methods to automatically classify *Allium* seed walls (anticlinal and periclinal). Figures 8–10 show the general results of the machine-based classifications. In these figures, we compared the machine-based and human-based methods. When more than three methods were combined for detecting the anticlinal wall, ST, S, and INS were the most predicted; UO, O, U were predicted to a medium level; and IC was the least predicted. In contrast, when more than four methods were combined, ST was the most predicted; INS, S, IC were predicted to a medium level; and UO, O, U were the least predicted. Lastly, more than five methods were combined, in which ST remained the most predicted.

Tables 5–7 show the classification results of each model. Here, most results are assumed to belong to different classes. Table 5 shows the results of predicting the anticlinal walls. The results suggested that most models considered IC and INS- types to be different, and GoogleNet and ResNet50 predicted the ST-type accurately. Table 6 shows the results of the classification of the periclinal walls using each model. CNN results show that GT and VT dominate. As shown in Table 6, ResNet50 and VGG16 predicted the GT-types accurately. Table 7 shows the performance of the combined models, in which most types are assumed to be IC-GT. These include U-VT, U-GT, U-LT, U-MT, IC-GT, O-VT, O-LT, O-MT, UO-GT, UO-VT, UO-LT, UO-MT, INS-GT, S-GT, S-VT, S-LT, ST-GT, ST-VT, ST-ST, ST-LT, and ST-MT.

When more than three methods are combined for the periclinal wall detection, GT, MT, and VT were the most predicted and ST, LT, and U were the least predicted. In contrast, when more than four methods were combined, VT was the most predicted, GT was the medium assumed, but MT, ST, LT were least predicted. The final prediction involved more than five cases, in which VT was the most predicted.

When more than three methods were combined, IC-GT had the highest prediction, ST-ST had a medium prediction, and ST-LT and INS-GT had the lowest prediction. In contrast, when more than four methods were combined, IC-GT continued to be the highest

**Table 7.** The SEM images of the anticlinal and periclinal walls classified by the five models (accuracy in percentages).

| | U-VT | U-GT | U-LT | U-MT | IC-GT | O-VT | O-LT | O-MT | UO-GT | UO-VT | UO-LT | UO-MT | INS-GT | S-GT | S-VT | S-LT | ST-GT | ST-VT | ST-ST | ST-LT | ST-MT |
|---|---|---|---|---|---|---|---|---|---|---|---|---|---|---|---|---|---|---|---|---|---|
| AlexNet results | | | | | | | | | | | | | | | | | | | | | |
| **IC-GT** | 100 | | 100 | 100 | **59** | 100 | 18 | | | | 100 | | 20 | 100 | 100 | 100 | 45 | | | | 50 |
| **O-MT** | | | | | | | | | | | | | 60 | | | | | | | | |
| **S-ST** | | 100 | | | 41 | | 82 | 68 | | | | | 20 | | | | 55 | 100 | 100 | | |
| **ST-VT** | | | | | | | | 32 | 100 | 100 | | 100 | | | | | | | | 100 | 50 |
| **CNN results** | | | | | | | | | | | | | | | | | | | | | |
| **IC-GT** | 100 | 100 | 100 | 100 | **49** | 100 | | | 100 | 100 | | | | 100 | | | | | | | 20 |
| **O-MT** | | | | | | | | | | | | | | | 100 | | | | | | |
| **S-ST** | | | | | 51 | | 48 | | | | 96 | | | | | | | 3 | | | |
| **S-LT** | | | | | | | | | | | | | | | | | **32** | | | | |
| **ST-GT** | | | | | | | 52 | | | | | | | | | | | | | | |
| **ST-VT** | | | | | | | | 100 | | | 4 | 100 | 100 | | | 100 | 68 | **97** | 100 | 100 | 80 |
| **GoogleNet results** | | | | | | | | | | | | | | | | | | | | | |
| **IC-GT** | 100 | 100 | 100 | 100 | **100** | 100 | | 70 | 100 | 100 | 100 | 100 | | 100 | 100 | 100 | 100 | 100 | 100 | 100 | 100 |
| **O-MT** | | | | | | | 100 | **30** | | | | | 80 | | | | | | | | |
| **S-ST** | | | | | | | | | | | | | 20 | | | | | | | | |
| **ResNet50 results** | | | | | | | | | | | | | | | | | | | | | |
| **IC-GT** | | 100 | | | **75** | | 70 | | 100 | | | | 3 | | | | | | | | |
| **O-VT** | | | | | 25 | | | | | | | | | | | | | | | | |
| **O-MT** | 100 | | | | | 100 | 30 | **40** | | 100 | 100 | 100 | 95 | 100 | | 50 | 100 | 100 | | 96 | |
| **S-GT** | | | | | | | | | | | | | 2 | | | | | | | | |
| **S-ST** | | | | 100 | | | | | | | | | | | | | | | | | |
| **S-VT** | | | | | | | | | | | | | | | | 50 | | | | | |
| **S-LT** | | | | | | | | | | | | | | | 100 | | | | | | |
| **ST-VT** | | | | | | | | 60 | | | | | | | | | | | | | |
| **ST-LT** | | | | | | | | | | | | | | | | | | | 100 | 4 | |
| **ST-MT** | | | 100 | | | | | | | | | | | | | | | | | | |
| **VGG16 results** | | | | | | | | | | | | | | | | | | | | | |
| **IC-GT** | | 100 | | | **100** | 100 | 100 | | 100 | 100 | | 51 | 100 | 100 | | | 50 | | | | 50 |
| **O-MT** | | | | 100 | | | | 100 | | | | | | | 100 | | | | | | |
| **S-ST** | | | | | | | | | | | | | | | | | | | | | |
| **S-VT** | 100 | | 100 | | | | | | | | 100 | | | | | | | | | | |
| **ST-VT** | | | | | | | | | | | | | | | | 100 | 50 | 100 | **100** | 100 | 50 |
| **ST-ST** | | | | | | | | | | | | 49 | | | | | | | | | |

**Table 8.** Counts of the anticlinal and periclinal walls.

| Anticlinal wall | | Periclinal wall | |
|---|---|---|---|
| Types | Count | Types | Count |
| IC | 3107 | GT | 14079 |
| INS | 2444 | MT | 7674 |
| O | 3410 | LT | 1848 |
| U | 3424 | ST | 5455 |
| UO | 4440 | VT | 3003 |
| S | 2273 | | |
| ST | 9045 | | |

predicted case, remaining types were least predicted. Therefore, more than five methods had no results obtained.

The percentage of results when more than three methods were combined was high in the anticlinal, periclinal, and combined wall classes, whereas the percentage of results when more than four or five methods were combined was low. However, ST was 100% for the anticlinal wall, GT was 81.9% for the periclinal wall, VT was 70.1%, ST-ST was 37.6% for the combined wall, IC-GT was 100% more effective than other walls; and ST-LT was 13.5%. Therefore, these

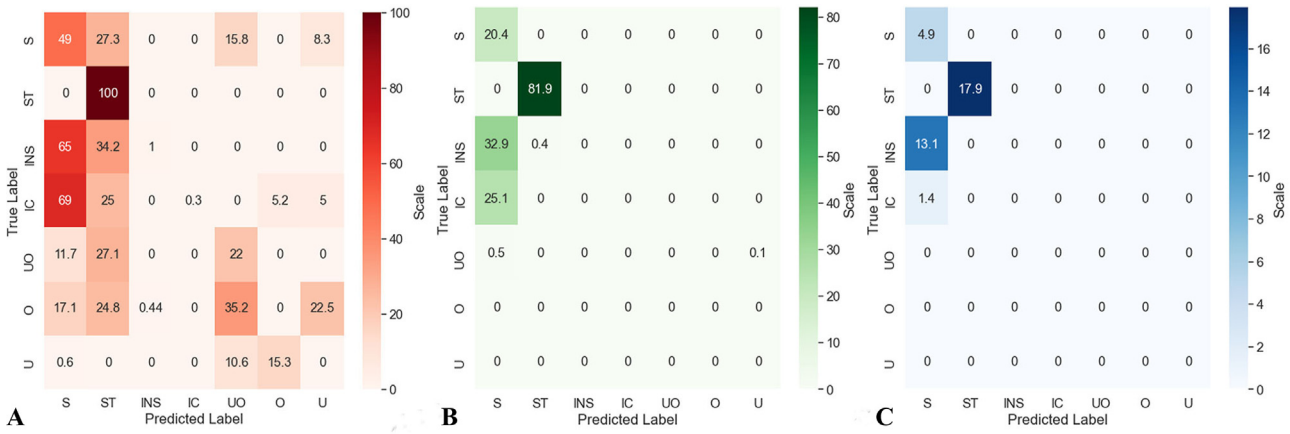


**Figure 8.** A, results of detecting the anticlinal wall using more than three methods; B, more than four methods; C, and more than five methods.

Please cite this article as: Ariunzaya G et al., Identification of seed coat sculptures using deep learning, Journal of Asia-Pacific Biodiversity, https://doi.org/10.1016/j.japb.2022.11.006

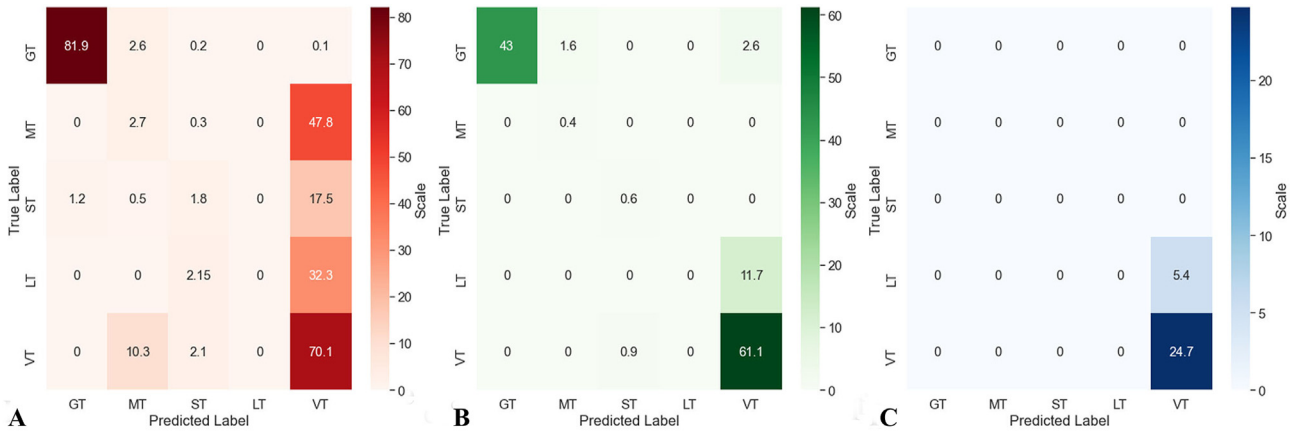


**Figure 9.** A, results of detecting the periclinal walls using more than three methods; B, more than four methods; C, and more than five methods.

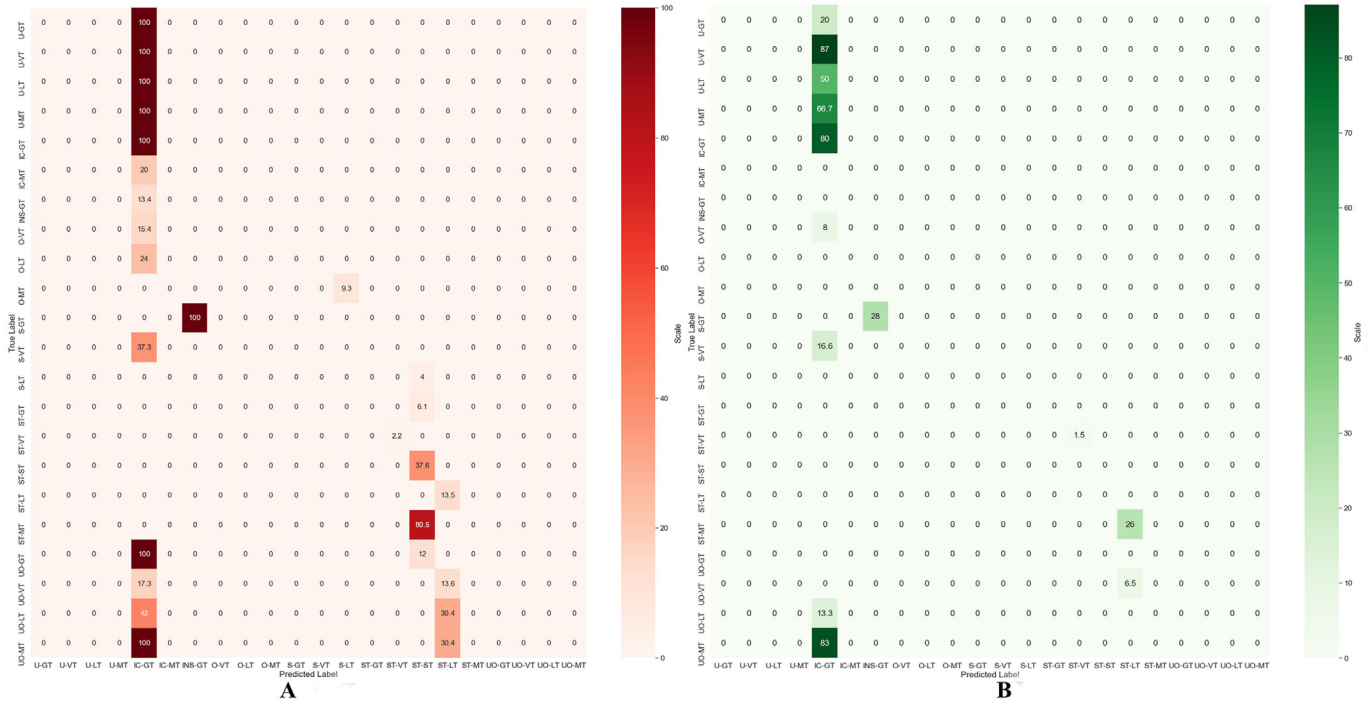


**Figure 10.** A, combined models containing more than three methods; B, more than four methods.

**Table 9.** The SEM images classified by the combined models.

| IC | | INS | | O | | U | | UO | | S | | ST | |
|---|---|---|---|---|---|---|---|---|---|---|---|---|---|
| Types | Count | Types | Count | Types | Count | Types | Count | Types | Count | Types | Count | Types | Count |
| IC-GT | 80 | INS-GT | 25 | O-VT | 235 | U-GT | 30 | UO-GT | 15 | S-GT | 300 | ST-GT | 1400 |
| IC-MT | 165 | | | O-LT | 150 | U-VT | 150 | UO-VT | 235 | S-VT | 75 | ST-VT | 550 |
| | | | | O-MT | 30 | U-LT | 310 | UO-LT | 150 | S-LT | 140 | ST-ST | 375 |
| | | | | | | U-MT | 140 | UO-MT | 70 | | | ST-LT | 184 |
| | | | | | | | | | | | | ST-MT | 1240 |

models were able to determine some macro and micromorphological properties of the *Allium* seed walls.

## Conclusions

In this study, we identified the seed coat sculptures of *Allium* species using ML methods for the first time. We trained five different network architectures namely, CNN, AlexNet, VGG16, GoogleNet, and ResNet50 for classifying *Allium* seed walls (anticlinal/periclinal) based on recognizing SEM images. We specially addressed the superiority of machine-based over human-based classification. The classification of *Allium* database containing seven types of anticlinal walls and five types of periclinal walls was studied. When more than three methods were combined, the best

Please cite this article as: Ariunzaya G et al., Identification of seed coat sculptures using deep learning, Journal of Asia-Pacific Biodiversity, https://doi.org/10.1016/j.japb.2022.11.006

results were obtained. Additionally, the highest accuracy of identifying periclinal walls was 98.1% obtained from VGG16. The anticlinal walls were predominantly identified as ST, S, O, and UO. The periclinal wall was predominantly identified as GT and VT. The results of combining more than three methods were better than those of combining more than four or five methods. Therefore, the models proved to be able to identify seed coat sculptures. In the future, we aim to improve the results obtained by combining the CNN architectural features to address the challenges of classifying *Allium* seed walls. Finally, we aim to realize a complete methodology that can integrate all the steps involved in this study, which focuses on classifying seed coat sculptures according to their characteristics. In the future, we have to study more species belonging to different genera within family or complicated taxonomic groups.

## Declaration of competing interest

The authors declare that they have no known competing financial interests or personal relationships that could have appeared to influence the work reported in this paper.

## Acknowledgments

This research was funded by the Korea Meteorological Administration Research and Development Program under Grant KMI 2021-01310. This study is a part of the M.S. thesis of the first author.

## References

Abbas I, Liu J, Amin M, et al. 2021. Strawberry fungal leaf scorch disease identification in real-time strawberry field using deep learning architectures. *Plants* 10:2643.

Antoniou A, Storkey A, Edwards H, et al. 2017. *Data augmentation generative adversarial networks*. Available at: arXiv preprint arXiv:1711.04340. [Accessed 12 November 2017]

Baasanmunkh S, Choi HJ, Oyuntsetseg B, et al. 2021. Seed testa sculpture of species of *Allium* L. (Amaryllidaceae) and its taxonomic implications. *Turczaninowia* 24:154–161.

Baasanmunkh S, Lee JK, Jang JE, et al. 2020. Seed morphology of *Allium* L. (Amaryllidaceae) from central Asian countries and its taxonomic implications. *Plants* 9:1239.

Banerjee K, Gupta RR, Vyas K, et al. 2020. Exploring alternatives to softmax function. *Computing Research Repository*:1–8. https://arxiv.org/abs/2011.11538.

Barthlott W. 1981. Epidermal and seed surface characters of plants: systematic applicability and some evolutionary aspects. *Nordic Journal of Botany* 1:345–355.

Bradley D, Roth G. 2007. Adaptive thresholding using the integral image. *Journal of Graphics Tools* 12:13–21.

Cadík M. 2008. Perceptual evaluation of color-to-grayscale image conversions. *Computer Graphics Forum* 27:1745–1754.

Celep F, Koyuncu M, Fritsch RM, et al. 2012. Taxonomic importance of seed morphology in *Allium* (Amaryllidaceae). *Systematic Botany* 37:893–912.

Choi HJ, Giussani LM, Jang CG, et al. 2012. Systematics of disjunct northeastern Asian and northern north American *Allium* (Amaryllidaceae). *Botany* 90:491–508.

Choi HJ, Oh BU. 2011. A partial revision of *Allium* (Amaryllidaceae) in Korea and north-eastern China. *Botanical Journal of Linnean Society* 167:153–211.

Davies E. 1990. *Machine vision: theory, algorithms and practicalities*. UK: Academic Press.

Dev S, Lee YH, Winkler S, et al. 2016. Color-based segmentation of sky/cloud images form ground-based cameras. *IEEE Journal of Selected Topics in Applied Earth Observations Remote Sensing* 10:231–242.

Duman H, Eksi G, Özbek F, et al. 2017. Two new species of *Allium* L. sect. *Allium* (Amaryllidaceae) from Turkey. *Plant Systematics and Evolution* 303:1271–1291.

Friesen N, Fritsch RM, Blattner FR, et al. 2006. Phylogeny and new intrageneric classification of *Allium* (Alliaceae) based on nuclear ribosomal DNA its sequences. *Aliso* 22:372–395.

Fritsch RM, Kruse J, Adler K, et al. 2006. Testa sculptures in *Allium* L. subg. *Melanocrommyum* (Webb and Berth.) Rouy (Alliaceae). *Feddes Repertorium* 117:250–263.

Ghimire B, Jeong MJ, Choi GE, et al. 2015. Seed morphology of the subfamily Helleboroideae (Ranunculaceae) and its systematic implication. *Flora* 216:6–25.

Golnabi H, Asadpour A. 2007. Design and application of industrial machine vision systems. *Robotics and Computer Integrated Manufacturing* 23:630–637.

Haralick RM, Shapiro LG. 1992. *Computer and robot vision*. Reading: Addision-Wesley.

He C, Liu J, Zhu Y, et al. 2021. Data augmentation for deep neural networks model in EGG classification task: a review. *Frontiers in Human Neuroscience* 15:765525.

He L, Chao Y, Suzuki K, et al. 2009. Fast connected-component labeling. *Pattern Recognition* 42:1977–1987.

Horng WB, Peng JW, Chen CY, et al. 2005. A new image-based real-time flame detection method using color analysis. *IEEE Networking Sensing and Control*:100–105.

Huang LK, Wang JJ. 1995. Image thresholding by minimizing the measures of fuzziness. *Pattern Recognition* 28:41–51.

Iwana BK, Uchida S. 2021. An empirical survey of data augmentation for time series classification with neural networks. *PLoS One* 16:e0254841.

Kanan C, Cottrell GW. 2012. Color-to-grayscale: does the method matter in image recognition? *PLoS One* 7:e29740.

Khalifa NE, Loey M, Mirjalili S, et al. 2021. A comprehensive survey of recent trends in deep learning for digital images augmentation. *Artificial Intelligence Review* 55:2351–2377.

Krizhevsky A, Sutskever I, Hinton GE, et al. 2017. ImageNet classification with deep convolutional neural networks. *Communication of the ACM* 60:84–90.

Kruse J. 1994. Rasterelektronenmikroskopische untersuchungen an samen der gattung *Allium* L. IV. *Feddes Repertorium* 105:457–471.

Li QQ, Zhou SD, He XJ, et al. 2010. Phylogeny and biogeography of *Allium* (Amaryllidaceae: Allieae) based on nuclear ribosomal internal transcribed spacer and chloroplast rps16 sequences, focusing on the inclusion of species endemic to China. *Annals of Botany* 106:709–733.

Lin CY, Tan DY. 2017. Seed testa micromorphology of thirty-eight species of *Allium* (Amaryllidaceae) from central Asia, and its taxonomic implications. *Nordic Journal of Botany* 35:189–200.

Liu X, Jiang S, Wu R, et al. 2022. Automatic taxonomic identification based on the fossil image dataset (>415,000 images) and deep convolutional neural networks. *Paleobiology*:1–22. https://doi.org/10.1017/pab.2022.14.

Mazur M, Marcysiak K, Dunajska A, et al. 2022. Taxonomic significance of seed morphology in *Veronica* L. (Plantaginaceae) species from central Europe. *Plants* 11:88.

McAndrew A. 2004. *An introduction to digital image processing with matlab*. Boston: Course Technology Press.

Pearson KD, Nelson G, Aronson MF, et al. 2020. Machine learning using digitized herbarium specimens to advance phenological research. *BioScience* 70:610–620.

Piazza G, Valsecchi C, Sottocornola G, et al. 2021. G. Deep learning applied to SEM images for supporting marine coralline algae classification. *Diversity* 13:640.

Reeb RA, Aziz N, Lapp SM, et al. 2022. Using convolutional neural networks to efficiently extract immense phenological data from community science images. *Frontiers in Plant Science* 12:787407.

Shorten C, Khoshgoftaar TM. 2019. A Survey on image data augmentation for deep learning. *Journal of Big Data* 6:1–48.

Singh TR, Roy S, Singh OI, et al. 2012. A new local adaptive thresholding technique in binarization. *International Journal of Computer Science Issues* 8:271–277.

Song JH, Hong SP. 2020. Fruit and seed micromorphology and its systematic significance in tribe *Sorbarieae* (Rosaceae). *Plant Systematics and Evolution* 306:1–14.

Veiskarami G, Khodayari H, Heubl G, et al. 2018. Seed surface ultrastructure as an efficient tool for species delimitation in the *Allium ampeloprasum* L. alliance (Amaryllidaceae, Allioideae). *Microscopy Research and Technique* 81:1275–1285.

Villaruz JA. 2021. Deep convolutional neural network feature extraction for berry trees classification. *Journal of Advances in Information Technology* 12:226–233.

Voulodimos A, Doulamis N, Doulamis A, et al. 2018. *Deep learning for computer vision: a brief review*. Computational Intelligence and Neuroscience 2018.

Wagle SA, Harikrishnan R, Ali SHM, et al. 2021. Classification of plant leaves using new compact convolutional neural network models. *Plants* 11:24.